Materials Advances

COMMUNICATION

View Article Online
View Journal | View Issue

Cite this: *Mater. Adv.*, 2022, 3, 8922

Received 3rd October 2022,
Accepted 16th October 2022

DOI: 10.1039/d2ma00949h

rsc.li/materials-advances

Crystallized glass tailored by controlled heat treatment for carbon dioxide capture under mild conditions†

Hyung-Ju Kim, *[a] Hee-Chul Yang, [a] Keunyoung Lee [a] and Richard I. Foster *[ab]

Described is the formation of crystallized alkaline earth oxide-containing glass adsorbents for radioactive carbon dioxide ($^{14}CO_2$) sequestering and mineralization under mild operating conditions; thus enabling the long-term geological disposal of hazardous ^{14}C. The best performing crystallized glass adsorbents recorded a max CO_2 capacity of 4.54 mmol g^{-1} and a carbonation reaction rate of 8.04 mmol g^{-1} h^{-1}.

Radioactive carbon dioxide ($^{14}CO_2$) capture using innovative materials is desirable due to associated radiological hazards,[1] and growing climate change.[2,3] In recent years, modified activated carbons,[4] metal–organic frameworks,[5,6] modified 3D graphene,[7] covalent organic frameworks,[8] and natural minerals[9] have been considered as adsorbents for CO_2. Mineral carbonation technology (MCT) is amenable to irreversibly capture CO_2, for example in the form of natural minerals,[9,10] or their mimics.[11,12] Typically, MCT is attractive because capturing carbon through the chemical reaction between alkaline earth metal ions and CO_2 forms insoluble and significantly stable carbonates.[13] However, most applications of MCT have an intrinsic restriction regarding their operational conditions since no forward reaction occurs within realistic time scales.[14] Thereby, the CO_2 capture performance, such as CO_2 capacity and carbonation reaction rate, of MCTs and their applications are severely restricted by the difficulty of operation under mild conditions. For example, natural minerals require aggressive carbonation reaction conditions *e.g.* high pressure ($\geq$20 bar), high temperature ($>$373 K), and pH-adjusted carrier solutions.[15] To overcome such obstacles, the fabrication of alkaline earth oxides impregnated into an amorphous glass structure have been recently developed.[16] They show enhanced rates of dissolution of alkaline earth metal ions and carbonation reaction due to the loosely packed glass structure and the generation of a surface coating silica gel, consequently facilitating CO_2 capture under mild conditions.[16]

Here, we report the synthesis and application of a crystallized glass tailored by controlled heat treatment for CO_2 capture under mild conditions. The controlled heat treatment of an alkaline earth oxide-containing glass gives rise to a structural transformation from amorphous to crystalline. The structural characterizations and CO_2 capture performance, including CO_2 capacity, carbonation reaction rate, and the dissolution rate of alkaline earth metal ion, were analyzed to reveal the impact of controlled heat treatment and phase transformation.

The materials used, fabrication procedures for amorphous glass, its crystallization, characterization, and CO_2 capacity measurement are described in detail in the ESI† (I. Materials and methods). An amorphous glass can be converted into the crystalline phase when heat-treated above its crystallization temperature, as demonstrated in Fig. S1 (ESI†). This crystallized glass is often referred to as glass-ceramic.[17] As shown in Fig. 1, the X-ray diffraction (XRD) pattern of the crystallized Sr-glass-Na_2O, prior to CO_2 capture, showed crystallinity including strontium oxide. These crystalline peaks were indexed as strontium metaborate (Joint Committee on Powder Diffraction Standards (JCPDS), SrB_2O_4: No. 15-0779). This definitive structure was previously reported as orthorhombic symmetry and *Pbcn* space group with a = 12.0135, b = 4.339, and c = 6.5864 Å.[18,19] After CO_2 capture, the structure of SrB_2O_4 was completely converted into the structure of $SrCO_3$ (JCPDS, No. 05-0418), which coincides well with the pattern in Fig. 1 without any remaining peaks from SrB_2O_4. That is to say, the crystallized Sr-glass-Na_2O reacted with CO_2 in the aqueous phase to form carbonates, and SrB_2O_4 is fully converted to $SrCO_3$.

The Fourier transform infrared attenuated total reflectance (FT-IR/ATR) spectroscopy of the 45 μm-sized crystallized Sr-glass-Na_2O

[a] *Decommissioning Technology Research Division, Korea Atomic Energy Research Institute, 989-111 Daedeok-daero, Yuseong-gu, Daejeon 34057, Republic of Korea. E-mail: hyungjukim@kaeri.re.kr*

[b] *Nuclear Research Institute for Future Technology and Policy, Seoul National University, 1 Gwanak-ro, Gwanak-gu, Seoul 08826, Republic of Korea. E-mail: rifoster@snu.ac.kr*

† Electronic supplementary information (ESI) available: Materials and methods, supporting figures, table. See DOI: https://doi.org/10.1039/d2ma00949h

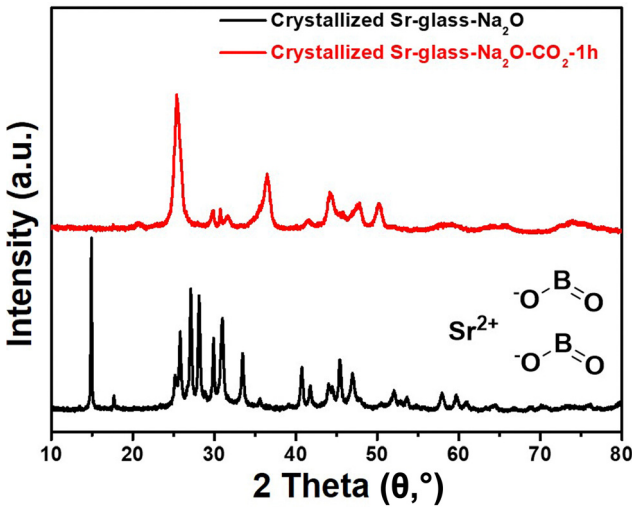

Fig. 1 XRD patterns of the crystallized Sr-glass-Na_2O (45 μm) prior and subsequent to 1 h of CO_2 capture at 298 K.

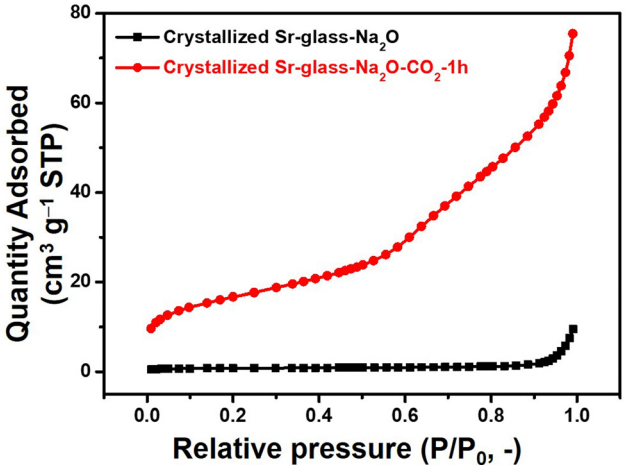

Fig. 3 N_2 adsorption isotherms at 77 K for crystallized Sr-glass-Na_2O (45 μm) prior and subsequent to 1 h of CO_2 capture at 298 K.

prior and subsequent to 1 h of CO_2 capture at 298 K was characterized as shown in Fig. 2a. The peaks near 1450 cm^{-1} (stretching vibration) and 850 cm^{-1} (bending vibration) visibly appear after CO_2 capture. The presence of these peaks indicates the formation of $SrCO_3$; an observation supporting the XRD patterns.[20] The C1s peaks near 290 eV in the X-ray photoelectron spectroscopy (XPS) intensified after 1 h of CO_2 exposure as shown in Fig. 2b, further confirming the capture and subsequent formation of carbonate.[21] Moreover, the N_2 physisorption revealed the textural properties of crystallized Sr-glass-Na_2O. As shown in N_2 adsorption isotherms (Fig. 3), the crystallized Sr-glass-Na_2O is absolutely a nonporous material classified by International Union of Pure and Applied Chemistry Type-II adsorption isotherm.[22] Subsequent to 1 h of CO_2 capture at 298 K, slight porosity is tailored due to the dissolved Sr from the material and newly produced $SrCO_3$. This is even more elucidated when the pore size distribution is analysed by Broekhoff-deBoer–Frenkel–Halsey–Hill method (Fig. S2, ESI†). Relative to the nonporous crystallized Sr-glass-Na_2O, the crystallized Sr-glass-Na_2O–CO_2 displays higher intensity in the mesopore (2–50 nm) range. The textural properties including Brunauer–Emmett–Teller (BET) surface area and pore volume are summarized in Table S1 (ESI†). Prior and subsequent to 1 h of CO_2 capture, the BET surface area increases from 1.43 to 51.13 $m^2\ g^{-1}$ and pore volume increases from 0.014 to 0.117 $cm^3\ g^{-1}$.

The CO_2 capacities of the crystallized Sr-glass-Na_2O was analyzed as a function of time. As shown in Fig. 4a, the maximum recorded CO_2 capacity was 4.54 mmol g^{-1} for crystallized Sr-glass-Na_2O after 3 h of reaction. Notably, CO_2 capacity after 12 h of reaction was exactly the same as that after 3 h based on the thermogravimetric analysis curve (Fig. S3, ESI†) which demonstrates that CO_2 capture was completed within 3 h, and the carbonation reaction was under equilibrium during the rest of the time. Crystallized Sr-glass-Na_2O had a higher capture efficiency (90.25%) and faster carbonation

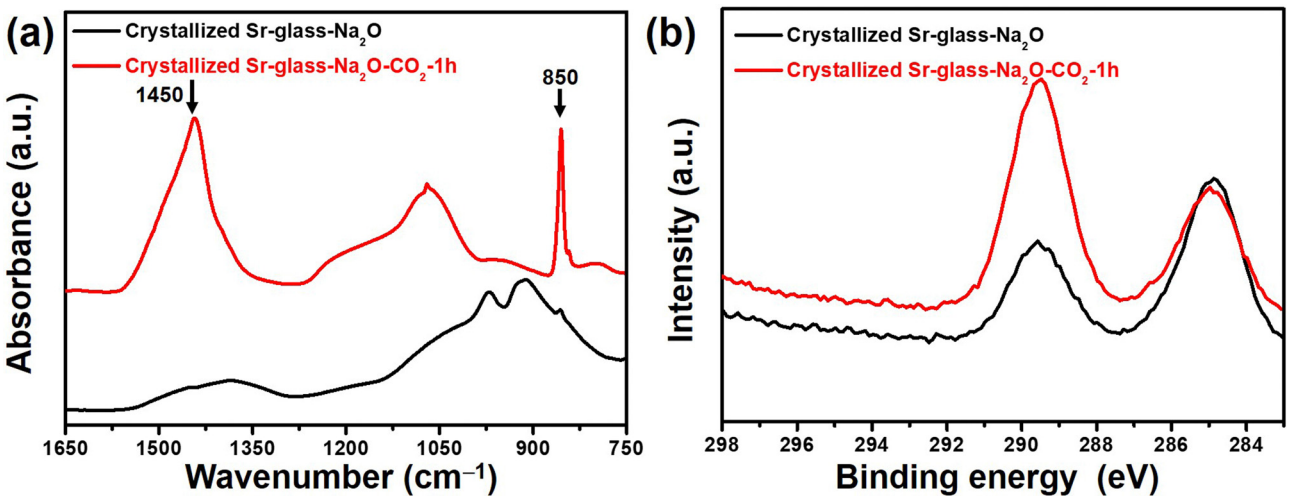

Fig. 2 (a) FT-IR/ATR absorption spectra, and (b) XPS C1s spectra of crystallized Sr-glass-Na_2O (45 μm) prior and subsequent to 1 h of CO_2 capture at 298 K.

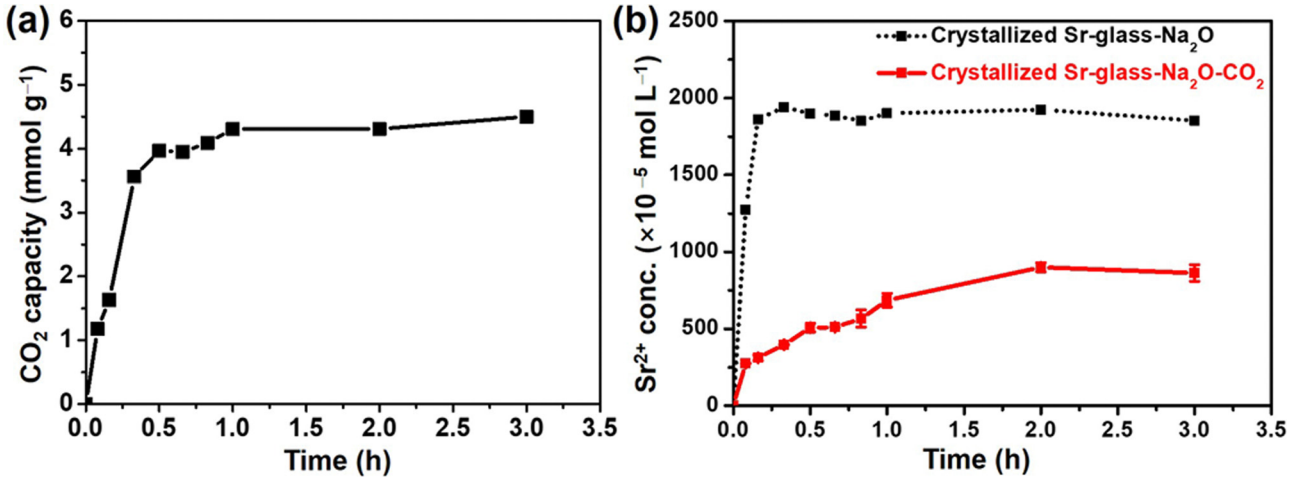

Fig. 4 (a) CO_2 capacity of crystallized Sr-glass-Na_2O (45 μm) and (b) equivalent molar concentrations of Sr^{2+} ion in the supernatant solutions under CO_2 flowing (solid black line) and CO_2 non-flowing (dotted red line) conditions at 298 K as a function of the reaction time.

reaction rate (8.04 mmol g^{-1} h^{-1} within 30 min) than our previously reported Sr-glass-Na_2O (88.07% and 7.25 mmol g^{-1} h^{-1}).[16] Efficiency calculations were performed as a ratio of the experimental and theoretical CO_2 capacities [experimental CO_2 capacity/theoretical CO_2 capacity × 100]. This improved performance is attributed to the enhanced dissolution of Sr^{2+} ion from the crystalline structure. Once the crystalline structure formed, most of the Sr^{2+} ions were present in the crystalline structure. Since most of the Sr^{2+} ions were gathered in the crystalline phase, they easily reacted on the specific sites and converted to $SrCO_3$. Thus, CO_2 capture performance was further improved comparing with amorphous Sr-glass-Na_2O which had evenly distributed Sr^{2+} ions in the structure. To further explain the observations, the Sr^{2+} dissolution rate, which is a rate-limiting step, was studied by inductively coupled plasma-optical emission spectroscopy analyzing the molar concentration of Sr^{2+} ions released from the crystallized glass under the conditions where CO_2 was either flowing or non-flowing as a function of the time (Fig. 4b). Notably, under the CO_2 non-flowing condition (dotted lines), crystallized Sr-glass-Na_2O possessed higher solubility than that of amorphous Sr-glass-Na_2O described elsewhere,[16] thereby almost 4 times higher (2000×10^{-5} mol L^{-1}) saturated concentration of Sr^{2+} ion. This coincides well with the advanced CO_2 capture performances (capacity, reaction rate and efficiency) of crystallized Sr-glass-Na_2O. The crystallized glass also exhibited the gradual increase of ion concentrations while CO_2 capture showed similar tendency as those of amorphous glass adsorbent, but the reaction rate and efficiency of crystallized Sr-glass-Na_2O were much higher than other glass adsorbents because of the enhanced Sr^{2+} ion solubility in water.

The CO_2 capture performance, max CO_2 capacity in mmol g^{-1} and CO_2 carbonation rate in mmol g^{-1} h^{-1}, of newly developed crystallized Sr-glass-Na_2O was compared with those of its amorphous glass adsorbent equivalent and other natural minerals under relatively mild CO_2 capture conditions reported previously (Table 1). As discussed, crystallized Sr-glass-Na_2O outperformed the precursor amorphous framework both in terms of CO_2 capacity and CO_2 carbonation rate with an almost doubling of performance. Even if natural minerals, such as serpentinite and wollastonite, containing alkaline earth metals (Mg and Ca), exhibited a superior max CO_2 capacity than crystallized Sr-glass-Na_2O, the aggressive CO_2 capture conditions (*i.e.*, energy intensive high temperature as well as acidic or

Table 1 Performance comparison of max CO_2 capacity and CO_2 carbonation rate of the crystallized Sr-glass-Na_2O with other lab-made or natural adsorbents capturing CO_2 *via* mineral carbonation mechanism under relatively mild temperature and pressure (1 bar) conditions

Mineral carbonation material	Max CO_2 capacity [mmol g^{-1}]	CO_2 carbonation rate [mmol g^{-1} h^{-1}]	Temperature [K]	Media	Ref.
Crystallized Sr-glass-Na_2O	4.54	8.04[a]	298	Deionized water	This work
Sr-glass-Na_2O	4.43	4.09[a]	298	Deionized water	16
Serpentinite	7.04	7.04	343	Orthophosphoric, oxalic, and ethylenediaminetetraacetic acid	23,24
Serpentinite	7.58	2.53	413	NH_4HSO_4/NH_3	25,26
Serpentinite	2.53	0.10	598	HCl/NaOH	27
Wollastonite	7	2.33	298	NH_4OH	28
Wollastonite	7.95	2.65	298	NH_4OH	29
Wollastonite	7.95	5.30	298	NH_4Cl/HCl	30

[a] CO_2 carbonation rate was obtained from the initial 1 h of CO_2 capture.

basic reaction media) were required as shown in Table 1. Nonetheless, the crystallized glass adsorbent fabricated in this work showed an extremely high initial CO_2 carbonation rate with a decent max CO_2 capacity even under moderate and favourable temperature, pressure, and media, where other natural adsorbents are not able to capture CO_2. For example, when the CO_2 capture was performed under room temperature (298 K) and atmospheric pressure (1 bar), the acidic and basic media were inevitably required to obtain a high CO_2 capacity for wollastonite,[28–30] and there was no report with such mild conditions when using serpentinite to the best of the authors' knowledge. In the crystallized Sr-glass-Na_2O, alkaline earth metal ions were more easily dissolved and captured CO_2 in comparison with natural minerals. This suggests that the appropriate support phase, here crystallized glass, as well as the incorporation of alkaline earth oxides make the highly efficient CO_2 capture feasible under mild capture conditions, which is applicable to $^{14}CO_2$ sequestration.

In conclusion, the fabrication of crystallized glass by restructuring *via* controlled heat treatment has been demonstrated; thereby implying better glass adsorbent for CO_2 capture than other MCT materials. The newly fabricated crystallized Sr-glass-Na_2O, also called SrB_2O_4, exhibits even higher performance in CO_2 capacity, carbonation rate, and efficiency due to the enhanced dissolution of alkaline earth metal ion; in this case Sr^{2+}. This development clearly suggests that the crystallized glass can be a technologically more desirable platform for long-term CO_2 capture, especially $^{14}CO_2$ disposal and storage security.

Hyung-Ju Kim: conceptualization, methodology, validation, formal analysis, investigation, writing – original draft, writing – review & editing, visualization. Hee-Chul Yang: resources. Keunyoung Lee: project administration. Richard I. Foster: writing – reviewing and editing.

Conflicts of interest

There are no conflicts to declare.

Acknowledgements

This work was supported by the National Research Foundation of Korea (NRF) grant funded by the Korea government (MSIP) (No. NRF-2022M2E9A2053685).

References

1 M. Lou Dunzik-Gougar and T. E. Smith, *J. Nucl. Mater.*, 2014, **451**, 328–335.
2 N. Abas and N. Khan, *J. CO_2* Util., 2014, **8**, 39–48.
3 P. Bains, P. Psarras and J. Wilcox, *Prog. Energy Combust. Sci.*, 2017, **63**, 146–172.
4 N. Abuelnoor, A. AlHajaj, M. Khaleel, L. F. Vega and M. R. M. Abu-Zahra, *Chemosphere*, 2021, **282**, 131111.
5 Z. Zhang, Q. Ding, S. B. Peh, D. Zhao, J. Cui, X. Cui and H. Xing, *Chem. Commun.*, 2020, **56**, 7726.
6 S. Shyshkanov, T. N. Nguyen, A. Chidambaram, K. C. Stylianou and P. J. Dyson, *Chem. Commun.*, 2019, **55**, 10964.
7 Y. Lin, Y. Tian, H. Sun and T. Hagio, *Chemosphere*, 2021, **270**, 129420.
8 Y. Huang, X. Hao, S. Ma, R. Wang and Y. Wang, *Chemosphere*, 2022, **291**, 132795.
9 S. Ó. Snæbjörnsdóttir, B. Sigfússon, C. Marieni, D. Goldberg, S. R. Gislason and E. H. Oelkers, *Nat. Rev. Earth Environ.*, 2020, **1**, 90–102.
10 A. Sanna, M. Uibu, G. Caramanna, R. Kuusik and M. M. Maroto-Valer, *Chem. Soc. Rev.*, 2014, **43**, 8049–8080.
11 I. M. Power, A. L. Harrison and G. M. Dipple, *Environ. Sci. Technol.*, 2016, **50**, 2610–2618.
12 O. Rahmani, *J. CO_2* Util., 2020, **35**, 265.
13 A. A. Olajire, *J. Pet. Sci. Eng.*, 2013, **109**, 364–392.
14 S. P. Veetil and M. Hitch, *Int. J. Environ. Sci. Technol.*, 2020, **17**, 4359–4380.
15 S. J. Gerdemann, W. K. O'Connor, D. C. Dahlin, L. R. Penner and H. Rush, *Environ. Sci. Technol.*, 2007, **41**, 2587–2593.
16 H.-J. Kim, S.-J. Kim, H.-C. Yang, H.-C. Eun, K. Lee and J.-H. Lee, *J. CO_2* Util., 2022, **61**, 102001.
17 R. D. Rawlings, J. P. Wu and A. R. Boccaccini, *J. Mater. Sci.*, 2006, **41**, 733–761.
18 P. D. Dernier, *Acta Cryst.*, 1969, **B25**, 1001–1003.
19 J. B. Kim, K. S. Lee, I. H. Suh, J. H. Lee, J. R. Park and Y. H. Shin, *Acta Cryst.*, 1996, **C52**, 498–500.
20 A. L. Vasiliu, M. V. Dinu, M. M. Zaharia, D. Peptanariu and M. Mihai, *Mater. Chem. Phys.*, 2021, **272**, 125025.
21 A. V. Shchukarev and D. V. Korolkov, *Cent. Eur. J. Chem.*, 2004, **2**, 347–362.
22 K. S. W. Sing, *J. Porous Mater.*, 1995, **2**, 5–8.
23 A. H. A. Park and L. S. Fan, *Chem. Eng. Sci.*, 2004, **59**, 5241–5247.
24 A. H. A. Park, R. Jadhav and L. S. Fan, *Can. J. Chem. Eng.*, 2003, **81**, 885–890.
25 X. Wang and M. M. Maroto-Valer, *ChemSusChem*, 2011, **4**, 1291–1300.
26 X. Wang and M. M. Maroto-Valer, *Fuel*, 2011, **90**, 1229–1237.
27 P. C. Lin, C. W. Huang, C. T. Hsiao and H. Teng, *Environ. Sci. Technol.*, 2008, **42**, 2748–2752.
28 W. Ding, L. Fu, J. Ouyang and H. Yang, *Phys. Chem. Miner.*, 2014, **41**, 489–496.
29 W. Ding, H. Yang, J. Ouyang and H. Long, *RSC Adv.*, 2016, **6**, 78090–78099.
30 H. Xie, F. Wang, Y. Wang, T. Liu, Y. Wu and B. Liang, *Environ. Earth Sci.*, 2018, **77**, 149.